RESEARCH IN APPLIED GEOPHYSICS

E M RESPONSE OF A RECTANGULAR THIN PLATE

BY

Y. LAMONTAGNE AND G.F. WEST

NO.2 FEB. 1971

GEOPHYSICS LABORATORY
DEPARTMENT OF PHYSICS
UNIVERSITY OF TORONTO

EM RESPONSE OF A RECTANGULAR THIN PLATE

by

Yves Lamontagne and G. F. West

This paper was presented at the 40th Annual Meeting of the Society of Exploration Geophysicists in New Orleans, on November 11, 1970. (Mining Session, paper M-21)

Department of Physics, Geophysics Division,
University of Toronto, Toronto 181, Canada.

ABSTRACT

By putting the fundamental equations in terms of the stream potential of the surface current density, it is possible to express the rectangular thin plate problem in a single equation subject to simple boundary conditions. A finite difference approximation of this equation reduces the problem to that of solving a large set of linear algebric equations. The solution of these equations by a modified Gauss-Seidel iterative method yields the stream potential and thus permits visualization of the eddy currents circulating inside the plate conductors. The secondary field calculated from the stream potential compares well with scale model measurements provided that the intervals used in the finite differences are small enough. Using a further approximation, inductively thick conductors can also be simulated if they are not also geometrically thick.

INTRODUCTION

The interpretation of EM prospecting surveys is chiefly based on knowledge of the theoretical response of the prospecting system to certain idealized models of possible geological conductors. In most cases, the theoretical responses have been obtained by laboratory measurements. The most notable exceptions are the sphere, the infinite slab, and the stratified half-space models for which a mathematical treatment is simpler than scale modeling. In the cases of the more realistic models such as the semi-infinite thin sheet (half-plane), only the solutions of special problems (e.g. perfect conductivity) have been found (Wesley, 1958; Wait, 1959; West, 1960). The thin sheet of finite extent has hardly been studied at all mathematically.

In order to further a study of the Turam system, the results of which are given in another paper (Lamontagne & West, 1971), we have attempted to calculate the response of a rectangular thin sheet by finite difference techniques. This method is especially well suited to a fixed transmitter geometry such as in employed in the Turam method, as there is only one transmitter-conductor geometry for all the

measurements of a survey. Thus only one finite difference solution is required for each case simulated, whereas a new solution would have to be calculated for each receiver position in the case of a moving transmitter system. Furthermore, the finite thin sheet is an especially useful model for Turam interpretation because of the important effect of conductor size on the Turam response. Nevertheless, the techniques to be described could be used for any fixed transmitter configuration for which the primary field is known over the surface of a thin conductor of finite extent. In the cases of moving source systems, it is possible to use the same computational method, but in general the computing cost would make it impractical.

THE PROBLEM

The problem which will be treated is precisely stated as the following: - to find, by numerical methods, the current system induced in a conducting, non-magnetic, rectangular plate which is subjected to an alternating magnetic field of known spatial variation (i.e. from a known source, such as a loop or dipole). The plate is situated in free space and the electromagnetic phenomena assumed to be quasistationary, i.e. to involve only induction, without propagation effects. The thickness of the

plate is assumed negligible compared to either the lateral dimensions of the plate or to the distance to the points where the magnetic field of the induced current system (secondary field) is calculated. The conductivity of the plate is assumed large, such that the surface conductivity is finite.

THEORETICAL BASIS

The problem must be formulated such that a single quantity describes the induced current system circulating inside the thin rectangular plate. We start with Maxwell's equations in the usual notation and using the rationalized MKS system of units:

$$\vec{\nabla} \times \vec{H} = \vec{J} + \frac{\partial \vec{D}}{\partial t} , \qquad (1)$$

$$\vec{\nabla} \times \vec{E} = -\frac{\partial \vec{B}}{\partial t} . \qquad (2)$$

For inductive problems, the $\frac{\partial \vec{D}}{\partial t}$ term of (1) can usually be neglected (see for example Grant & West, 1965, chapter 16) so that (1) can be written as:

$$\vec{\nabla} \times \vec{H} = \vec{J} . \qquad (3)$$

There are also the empirical relations:

$$\vec{B} = \mu \vec{H} , \qquad (4)$$

$$\vec{J} = \sigma \vec{E} . \qquad (5)$$

Since the divergence of the curl is identically zero, (2) and (3) yield:

$$\vec{\nabla} \cdot \vec{J} = 0 , \qquad (6)$$

$$\vec{\nabla} \cdot \vec{B} = 0 .$$

To express the problem in terms of the current density $\vec{J}$, let us first substitute $\vec{E}$ from equation (5) and $\vec{B}$ from equation (4) into (2). Thus, for a sinusoidally varying source field of angular frequency ω and assuming a uniform medium, one obtains:

$$\vec{\nabla} \times \vec{J} = -i\sigma\mu\omega \vec{H} . \qquad (7)$$

Then $\vec{H}$ in (7) can be eliminated using the integral form of equation (3) (the Biot-Savart equation). The resulting equation is:

$$\vec{\nabla} \times \vec{J}(\vec{r}_0) = -i\sigma\mu\omega \int_V \frac{\vec{J}(\vec{r}) \times (\vec{r} - \vec{r}_0)}{4\pi |\vec{r} - \vec{r}_0|^3} d^3r , \qquad (8)$$

where V includes all regions where current flows.

The integral in equation (8) has two contributions. One is that of the transmitter current and the other that of the induced current. Since the contribution of the transmitter is easily evaluated, let us replace it by the known

function $\vec{P}(\vec{r}_o)$. The equation obtained is:

$$\vec{\nabla} \times \vec{J}(\vec{r}_o) = -i\sigma\mu\omega \left\{ \vec{P}(\vec{r}_o) + \int_C \frac{\vec{J}(\vec{r}) \times (\vec{r} - \vec{r}_o)}{4\pi |\vec{r} - \vec{r}_o|^3} \right\}, \quad (9)$$

where C indicates that the integral is to be evaluated in the region occupied by the conductor.

"INDUCTIVELY THIN" CONDUCTORS

If a plate conductor is thin enough(1), the current density can be considered constant across the thickness (condition A). In this case, one can use the surface current density defined as:

$$\vec{K} = \int_{-t/2}^{t/2} \vec{J}\, dx = \vec{J}t,$$

where x is the direction along which the thickness t is measured (see Figure 1).

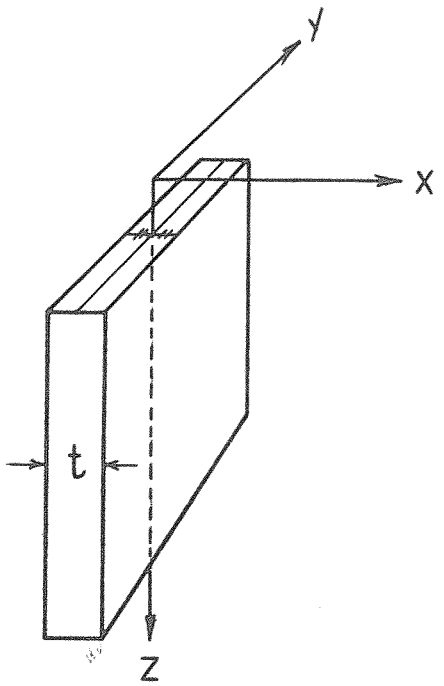

Fig. 1. Coordinate system. The coordinate system is attached to the conductor. The thickness t is measured along the x axis and is small.

(1) See section on inductively thick conductors for a definition of this condition.

Substituting the surface current density for $\vec{J}$ in (9) yields:

$$\vec{\nabla} \times \vec{K}(\vec{r}_0) = -i\sigma\mu\omega t \left\{ \vec{P}(\vec{r}_0) + \int_S \frac{\vec{K}(\vec{r}) \times (\vec{r} - \vec{r}_0)}{4\pi |\vec{r} - \vec{r}_0|^3} d^2r \right\}. \quad (10)$$

This last equation is obtained by assuming that t is geometrically small so that $\{(\vec{r} - \vec{r}_0)/|\vec{r} - \vec{r}_0|^3\}$ does not vary appreciably across the thickness (condition B). The conditions A and B would be perfectly respected only by an infinitely thin conductor of finite conductivity-thickness product, but in practice the approximation is good within fairly broad limits including a good proportion of geologically occuring conductors.

THE STREAM POTENTIAL

The only equations needed to solve for $\vec{K}$ are equation (10) and an equation derived from (6):

$$\vec{\nabla} \cdot \vec{K} = 0. \quad (11)$$

This divergence equation (11) can be eliminated by using a vector potential $\vec{U}$ such that

$$\vec{\nabla} \times \vec{U} = \vec{K}, \quad \text{and} \quad \vec{\nabla} \cdot \vec{U} = 0.$$

Replacing $\vec{K}$ by $\vec{\nabla} \times \vec{U}$ and using the identity $\vec{\nabla} \times \vec{\nabla} \times \equiv (\vec{\nabla} \nabla \cdot - \nabla^2)$, (10) then becomes:

$$\nabla^2 \vec{U}(\vec{r}_0) = i\sigma\mu\omega t \left\{ \vec{P}(\vec{r}_0) + \int_S \frac{(\vec{\nabla}\times\vec{K}(\vec{r}))\times(\vec{r}-\vec{r}_0)}{4\pi|\vec{r}-\vec{r}_0|^3} d^2r \right\}, \qquad (12)$$

in rectangular coordinates. If the coordinates are chosen as in Figure 1, only the x component of $\vec{U}$ exists (under the conditions stated above). U_x can be considered as a scalar function of the two variables y and z. It can be visualized as the stream potential of the current circulating inside the plate, and its units are amperes. Thus dropping the subscript, contours of U are the flow lines of the induced eddy currents. The scalar form of (12) is:

$$\nabla^2 U(y,z) = i\sigma\mu\omega t \left\{ P_x(y,z) + \int_S \frac{\vec{\nabla}U_0 \cdot (\vec{r}-\vec{r}_0)}{4\pi|\vec{r}-\vec{r}_0|^3} d^2r \right\}. \qquad (13)$$

In terms of the stream potential, the boundary conditions are easily expressed as U = constant everywhere on the edge of the plate. Since only the derivatives of U enter the equation (13), this condition can be stated U=0 on the edge of the plate.

This is the only boundary condition and, together with (13), it completely defines the problem.

FINITE DIFFERENCE EQUATION

The finite difference formulation is obtained by laying a rectangular grid over the surface of the plate as illustrated in Figure 2 and by approximating differentials by

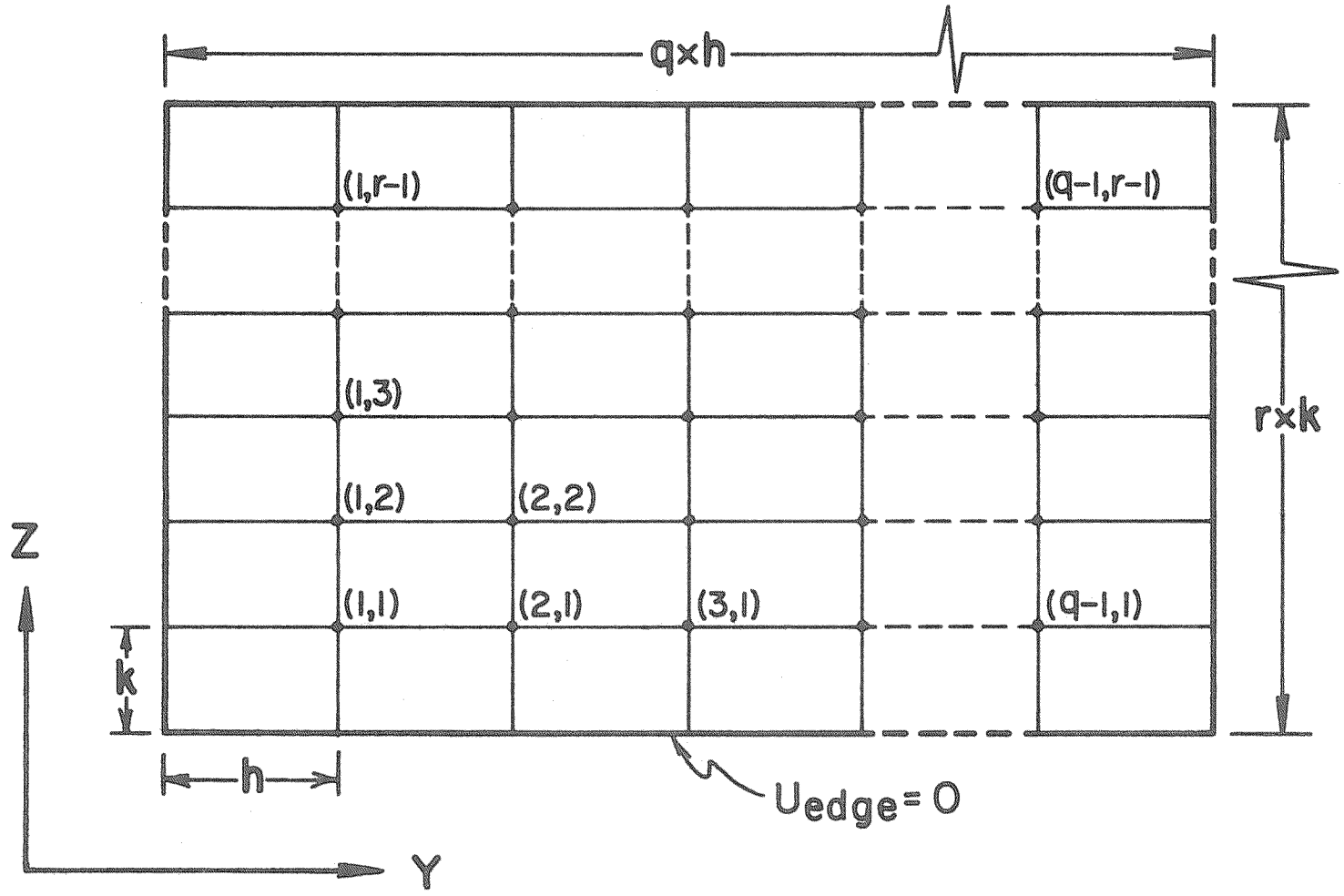

FIG 2. The finite difference grid. There are q times r grid elements of size h by k. The x component of the primary field P is specified by its $p_{i,j}$ values at the (q-1)(r-1) interior grid intersections. The problem consists in calculating the $u_{i,j}$ values of the stream potential U at the same intersections.

differences and integrals by summations. Various finite difference forms are derived depending on the degree of sophistication used in the approximations. In the case of a square grid, the simplest form is:

$$u_{m+1,n} + u_{m-1,n} + u_{m,n+1} + u_{m,n-1} - 4\,u_{m,n} = i\sigma\mu\omega t k\left\{k.p_{m,n} - \sum_{i=1}^{q-1}\sum_{j=1}^{p-1}\left[\frac{(u_{i,j}-u_{i+1,j})(i+1/2-m)}{4\pi\left[(i+1/2-m)^2+(j-n)^2\right]^{3/2}} + \frac{(u_{i,j+1}-u_{i,j})(j+1/2-n)}{4\pi\left[(i-m)^2+(j+1/2-n)^2\right]^{3/2}}\right]\right\} \quad (14)$$

This form is useful only as an illustration since the crude approximation of the integral of equation (13) produces singularities. In the general case, one can express the Laplacian operator and the integral as linear operations. Putting:

$$\nabla^2 U \approx [D]\,U,$$

and

$$\int_S \frac{\vec{\nabla}U_o.(\vec{P}-\vec{P}_o)}{4\pi\,|\vec{P}-\vec{P}_o|^3}\,d^2P \approx [C]\,U,$$

one can express the equation (13) in matrix notation as:

$$[D]\,U = i\sigma\mu\omega t k\,(k.P + [C]\,U). \quad (15)$$

In this equation, U and P are two-dimensional matrices whereas [D] and [C] are four dimensional transformation matrices.

a) Laplacian operator. The Laplacian operator can be approximated by various finite difference expressions depending on the order of the approximation. Since the transformation matrix [D] is four-dimensional, it is impossible to display it directly. The simplest representation is by means of "star diagrams". Two operators are represented by such diagrams in Figure 3. The first one (A) is precise to the third order and the second (B) to the fifth order. By centering a star diagram at a grid point (m,n) (evaluating the Laplacian at (m,n) as part of equation (m,n)), one obtains the non-zero elements $d_{m,n,i,j}$ of [D] by coincidence of the nodes of the star with the grid points (i,j). The matrix [D] can be considered two-dimensional if (m,n) is denoted by s and (i,j) by v according to the relations:

$$s = (n-1)(q-1) + m,$$

$$v = (j-1)(q-1) + i,$$

where q and r are the numbers of grid intervals in y and z respectively. It can then be roughly visualized as having all zero elements except five diagonals, although this is not true in details because of boundary effects. In this case, U would be considered as a vector with elements u_v.

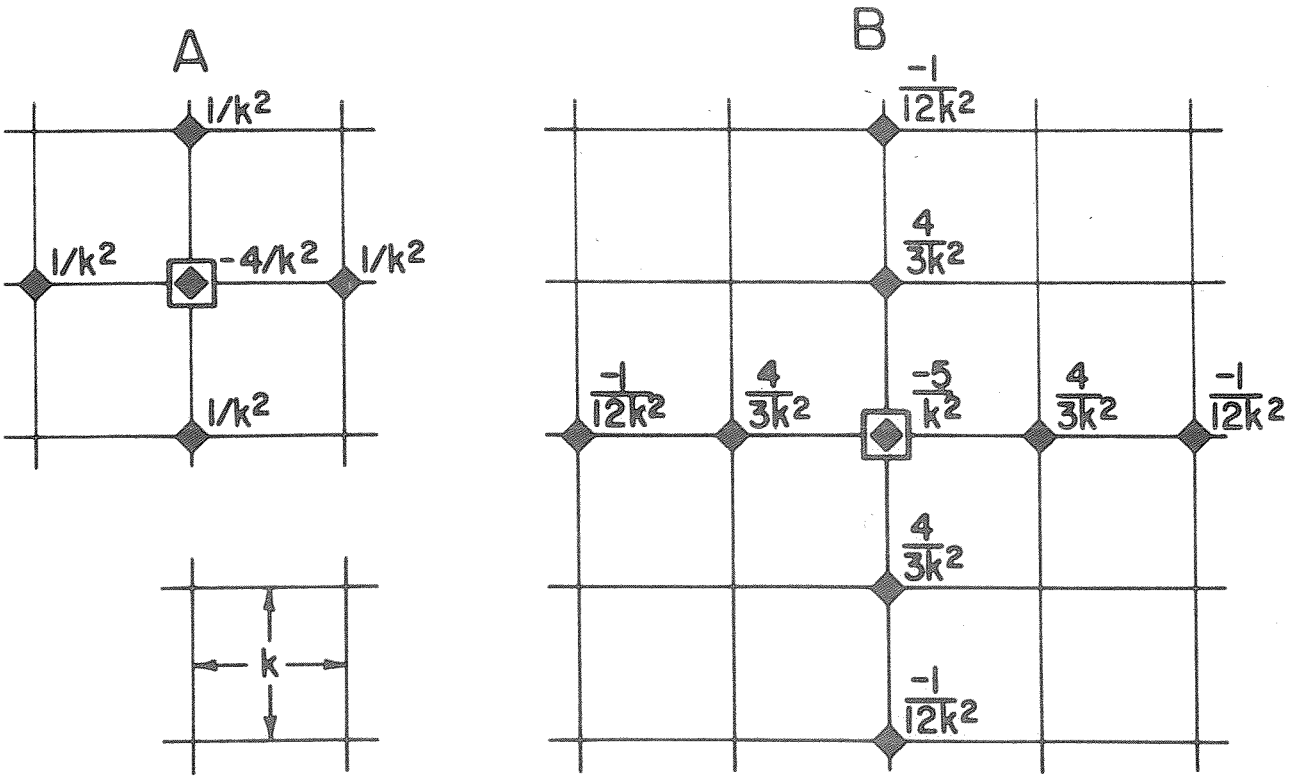

FINITE DIFFERENCE APPROXIMATIONS OF ∇^2

FIG 3. "Star diagrams" for two finite difference approximations of $(\partial^2/\partial y^2 + \partial^2/\partial z^2)$. A is a 3^{rd} order approximation and B a 5^{th} order approximation. The diagram is used by superposing it on the finite difference grid with the centre (denoted by a square) at the point where the Laplacian is to be found. The lozenges indicate the non-zero elements of the operator which act as coefficients of the corresponding grid values of U in the linear combination.

b) Integral. The integral of equation (13) is approximated by the linear transformation:

$$S = [C]\, U ,$$

where S and U are two-dimensional matrices and [C] a four-dimensional matrix. At a point (m,n), the evaluation of the integral is:

$$s_{m,n} = \sum_{i=1}^{q-1} \sum_{j=1}^{r-1} c_{m,n,i,j} \cdot u_{i,j} .$$

The $c_{m,n,i,j}$ elements can be calculated by considering expressions such as:

$$(D_y u)_{m+1/2,\,n} = (u_{m+1} - u_{m,n})/h ,$$

$$(D_z u)_{m,\,n+1/2} = (u_{m,n+1} - u_{m,n})/k ,$$

from which can be formed the quadrature approximation of $\vec{\nabla} U$:

$$\vec{\nabla} U(y,z) \approx \sum_{i=1}^{q-1} \sum_{j=1}^{r-1} \left\{ (D_y u)_{m+1/2,\,n} \cdot T(y/h - i + 1/2,\, z/k - j) - (D_z u)_{m,\,n+1/2} \cdot T(y/h - i,\, z/k - j - 1/2) \right\}$$

where:

$$T(y,z) = (1-|y|)(1-|z|) , \qquad |y| \le 1, \text{ and } |z| \le 1 ;$$

$$T(y,z) = 0 , \qquad |y| > 1, \text{ or } |z| > 1 .$$

And at a point (m,n), the integral can then be expressed as:

$$\mathcal{S}_{m,n} \approx \sum_{i=1}^{q-1}\sum_{j=1}^{r-1}\left\{ (u_{i+1,j}-u_{i,j}) \int_{-h}^{h}\int_{-k}^{k} \frac{(1-|y/h|)(1-|z/k|)\{(m-\tfrac{1}{2}-i)h+y\}\,dy\,dz}{h\left[\{(m-\tfrac{1}{2}-i)h-y\}^2+\{(n-j)k-z\}^2\right]^{3/2}}\right.$$

$$\left. -(u_{i,j+1}-u_{i,j}) \int_{-h}^{h}\int_{-k}^{k} \frac{(1-|y/h|)(1-|z/k|)\{(n-\tfrac{1}{2}-j)k+z\}\,dy\,dz}{k\left[\{(m-i)h-y\}^2+\{(n-\tfrac{1}{2}-j)k-z\}^2\right]^{3/2}}\right\}. \qquad (16)$$

Since each grid value of $u_{i,j}$ is involved in 4 terms of the summation, each $c_{m,n,i,n}$ element is an algebraic sum of 4 definite integrals such as those on the right of (16), which can be evaluated analytically. This approximation of the integral (13) is the simplest one which produces no singularity at m=1 or n=j, and such that the total amount of current is conserved. Furthermore, it has the advantage that the elements of matrix [C] are evaluated in the same way everywhere in the matrix, including those corresponding to points near the boundary.

Higher order approximations can be obtained using truncated polynomials of 3rd degree, 5th degree, etc.... If these are used, a correspondingly more refined approximation of the Laplacian operator must be used. In the case of 3rd degree truncated polynomials, for example, each $c_{m,n,i,j}$ is evaluated as a sum of 16 integrals similar to those of equation

(16). But such a more refined scheme does not necessarily yield a more accurate solution, as will be seen in a later discussion.

SOLUTION OF THE LINEAR SYSTEM

Rearranging equation (15) in the form:

$$[D - i\sigma\mu\omega tkC]U = i\sigma\mu\omega tk^2P$$

or:

$$[A]U = B,$$

it is realized that the problem is now reduced to that of solving the (p-1)(q-1) linear algebraic equations to obtain the values of the stream potential U at the grid points. Figure 4 is a visualization of one such finite difference equation applied at one of the (p-1)(q-1) points. By applying a similar equation at every grid point (except those on the boundary), the matrix A is formed. It can be seen that it is a full matrix (i.e. having no zero element). This is an uncommon result in finite difference problems, and constitutes the main difficulty of the linear problem. In the case of a 11 by 11 grid for example, there are 100 unknowns and the matrix [A] contains 10,000 complex elements. Subdividing the grid by two produces a matrix of 160,000 complex elements, too large for the core storage available on most computers.

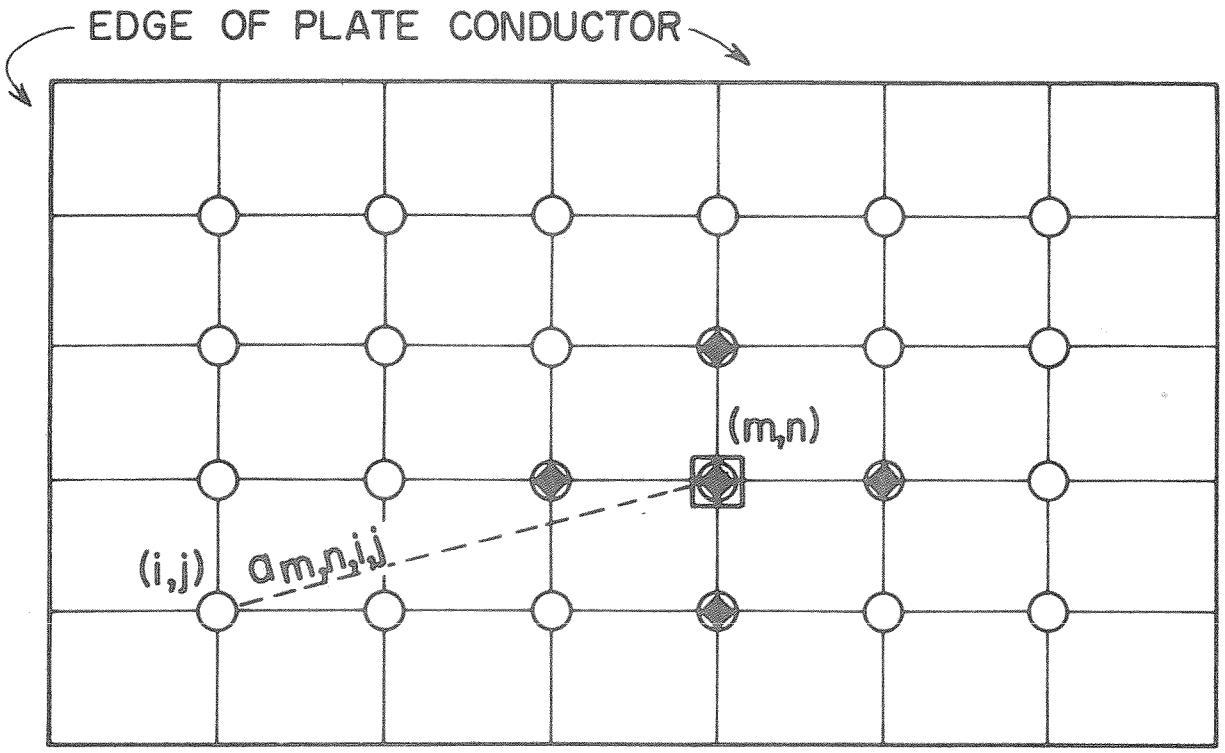

□ POINT WHERE THE EQUATION IS APPLIED: (m,n)

○ POINTS CONTRIBUTING TO THE INTEGRAL PART

◆ POINTS OF THE LAPLACIAN OPERATOR

$$\sum_i \sum_j (a_{m,n,i,j} \cdot u_{i,j}) - p_{m,n} = 0$$

FIG 4. Diagrammatic representation of how the stream potential values $u_{i,j}$ at the different grid points contribute to the finite difference equation (17). The coefficients of the integral part are imaginary; those of the Laplacian are real.

Thus only the problems of relatively small size (i.e. coarse grid) can be solved by standard complex linear equation solvers. The limitations are of many kinds: 1) the required computing time grows as the cube of the number of unknowns; 2) the whole array A must be stored in high speed core storage because it is constantly operated upon; 3) the large number of accumulated truncation errors adversely affects the precision of the solution unless double precision arithmetic is extensively used (a further expense in computing time). On the IBM 360/65, this sets the practical limit at roughly 150 grid points, which corresponds to a grid of 11 by 16 intervals. Since a finer grid was judged necessary for most cases, a successive approximation method was devised to solve the simultaneous equations. It is a modification of the Gauss-Seidel method (see for example Isaacson & Keller, 1966, p.66ff) and requires that the matrix [A] be diagonally dominant. The modification was necessary because of the slow convergence of the direct process, a consequence of the fact that the matrix is diagonally dominant only in a marginal way.

The technique used consisted in assuming initial grid point values for U and calculating the residuals(2):

$$r_i = b_i - \sum_m a_{i,m} u_m .$$

---

(2) In the following, [A] is considered a two-dimensional matrix and R, B, U are vectors.

The next trial value of u_i is then calculated as:

$$u_i + (g \cdot r_i)/a_{i,i},$$

g being a coefficient adjusted to optimize the convergence to the true solution. The next trial value calculated is that of u_{i+1}, the latest values of the other u_m's being used to evaluate r_{i+1}. In each iteration, all the grid values of U are replaced by better approximations and the process is repeated until all the normalized residuals ($r_i/a_{i,i}$) are smaller than a specified fraction of the average u value. When this fraction is set to 10^{-5}, the true solution of the linear equation problem is normally attained within a relative error of less than 10^{-4} (with normal convergence).

The matrix [A] is not modified by the iterative process. In consequence, it does not have to be stored explicity. It is easily reconstituted from two separate tables of much smaller size since:

$$a_{m,n,i,j} = f_{|m-i|,|n-j|} + i\, e_{|m-i|,|n-j|},$$

where F has only 5 non-zero elements and E is a real, tabulated function of (q-1)(r-1) elements instead of the $\{(q-1)(r-1)\}^2$ complex elements of the matrix [A]. This is true only for the

low order approximations described above. A few more similar tables are required for approximations including higher order terms, but the saving of storage is still very substantial.

The convergence of the iterative process is affected by the parameters of the problem solved. For problems with the same number of grid points, the convergence increases when the $\sigma\mu\omega t k$ product is larger. On the other hand, as will be seen later, the finite difference solution usually deviates more from the true solution when this product is larger. Thus in practice, a compromise must be made between a fast convergence and a good accuracy.

Another factor having an important effect on the convergence is the acceleration coefficient g. In the cases of large problems, this coefficient can be made self-adjusting by means of an algorithm which examines the successive variations of the residuals and determines amplitude and phase corrections to be applied to it (it has a complex value).

The resulting program are particularly efficient for solving sequences of EM configurations where the parameters vary in gradual steps. This is ideal for simulating a series of conductors of varying conductivities, dips, depths, etc... In these cases, it is possible to use the previous solution

and acceleration coefficient as a starting point for the next problem of the sequence. When only one situation is simulated, a similar increase in efficiency can be achieved by using a larger $\sigma\mu\omega t$ value for the first few iterations and gradually decreasing it to the actual value of the problem. This brings about a faster convergence to the true solution and a fast adjustment to the optimum acceleration coefficient.

Several computer programs were written using variations of the basic algorithm. Later versions incorporated the various improvements just described, plus other modifications aimed at at liquidating the residuals faster by altering the order and frequency with which the different grid points are relaxed. The method is so flexible that there is still a virtually unlimited number of improvements which can be added to the basic scheme without endangering the accuracy and soundness of the process. The reason for this adaptability is that any method that helps to decrease the residuals cannot be in error, since the right solution must be obtained when the residuals are reduced to zero. This presupposes that the [A] matrix is well conditioned, but this in indicated by the fact that it is diagonally dominant. Another test of the generality of the

matrix is the good stability in the solutions obtained with slightly different [A] matrices (e.g. when different approximation schemes are used).

There are some cases when the iterative process may become divergent. These cases occur when higher order approximations are used (such as the 9 point star of figure 3B together with the 3rd order quadrature approximation for the inte gral). This behavior arises only for certain values of the $\sigma\mu\omega tk$ parameter. It is possible that the polynomial representation implied is too strict and is unsuitable for the functional variation of the stream potential. It is suspected that the difficulty lies with the high order "star" rather than with the approximation of the integral since these star diagrams correspond to matrices which are not diagonally dominant in the strict sense.(3)

The best performance is generally attained using the simpler approximation described above (including the 5 point "star" of figure 3A, except with a rectangular non-square grid). As an example, a problem of 400 unknowns can be solved in an average time of less than 5 minutes on the IBM 360/65 computer whereas the time required by a standard complex linear solver

---

(3) When the modulus of a diagonal element is not larger or equal to the sum of moduli of the other row or column elements.

would be approximately 30 minutes.(4) Symmetrical problems of 884 points have been solved in a comparable time (6 minutes) by a version of the same algorithm using the mirror image symmetry to reduce the number of independant unknowns.

EXAMPLES OF CALCULATED RESPONSES

Stream potential maps

The stream potential U can be used directly to display the eddy current in a plate conductor. This is done by contouring the real and imaginary parts of U in the yz domain (i.e. the plane containing the conducting plate). Figures 5 and 6 show such stream potential maps. The rectangular outlines are the edges of the plates. The geometries of the cases calculated are sketched on the right of Figures 7 and 8 respectively: these are fairly common situations encountered in Turam surveys, as suggested by the list of parameters which would lead to these responses.

The example of Figure 6 displays an unexpected quadrature current pattern. The response is that of a good conductor, as will be seen in Figure 8. The pattern can be explained as due to an over-cancellation of the primary field by the secondary

---

(4) Provided that the 320,000 words of fast core storage were available and a precise solution could be obtained in single precision arithmetic.

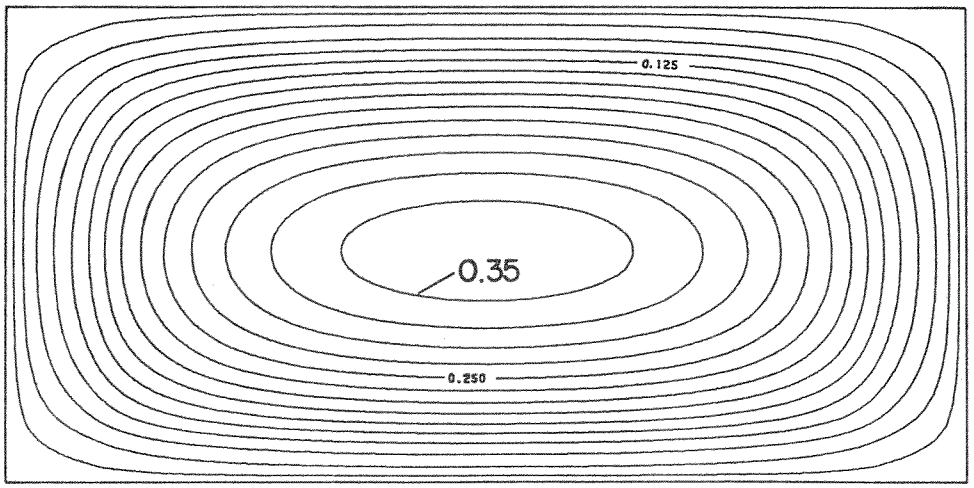

IN PHASE COMPONENT — INTERVAL = 0.025 AMP.

EDDY CURRENT PATTERN

FOR LOW Q RESPONSE: Q = 1.08

QUADRATURE COMPONENT — INT. = 0.025 AMP.

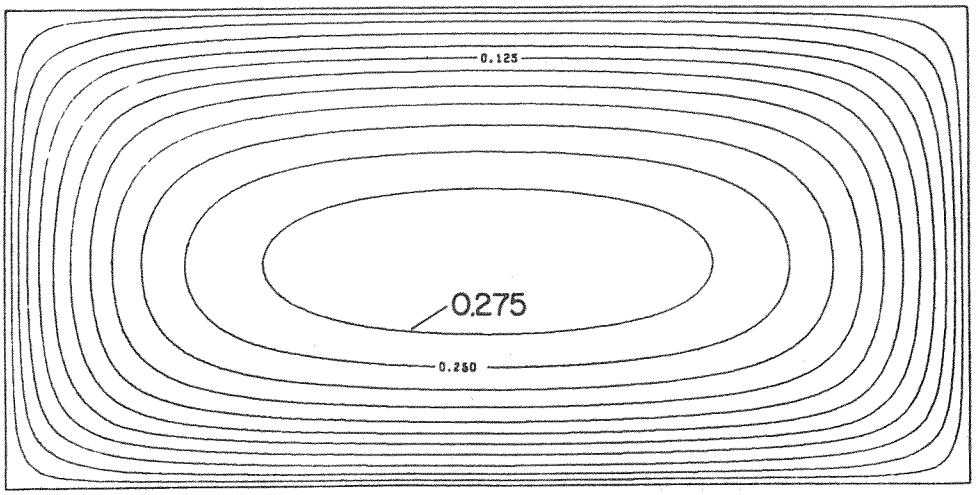

FIG 5. Eddy current pattern for the conductor shown on the right side of Figure 7. The response is that of a relatively poor conductor as indicated by the low Q (ratio of maximum in phase to quadrature amplitudes of the surface anomaly). The number of grid points in y and z is 15 by 15.

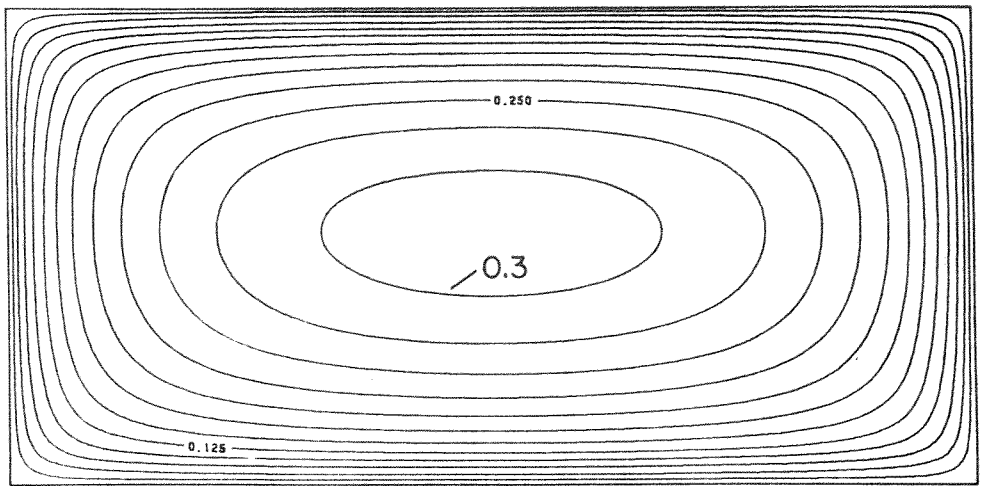

IN PHASE COMPONENT INTERVAL = 0.025 AMP.

EDDY CURRENT PATTERN

FOR HIGH Q RESPONSE: Q = 5.64

QUADRATURE COMPONENT INTERVAL = 0.005 AMP.

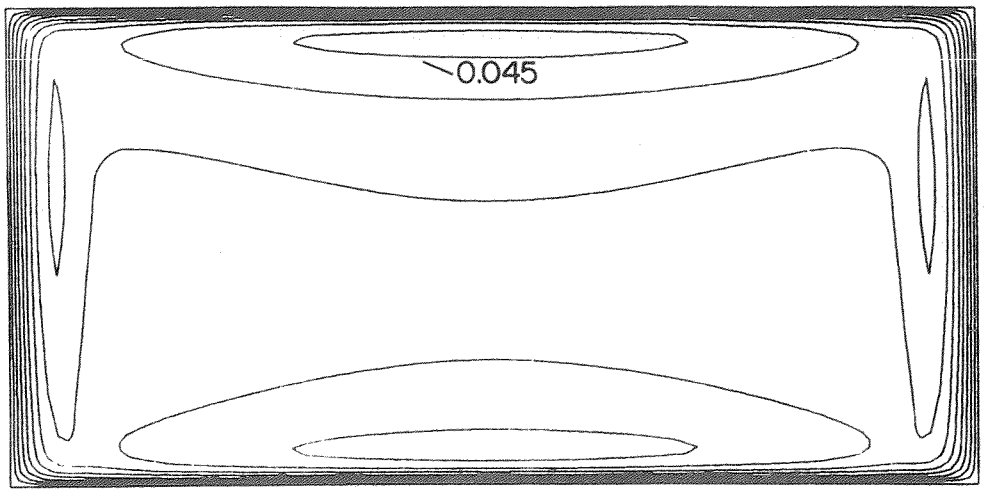

FIG 6. Calculated in phase and quadrature eddy currents for a relatively good conductor (high Q response). The geometry and parameters are shown on the right side of Figure 8. The number of grid intervals is 25 in y and 33 in z.

field in the central portion of the conductor where the stream potential has a concave surface.

Calculated anomalies

Once the stream potential of the current is known, it is a simple matter to calculate the secondary field produced in the surroundings of a conductor. This is done by digital integration of the induced currents using Biot-Savart equation. But some care must be taken to use a proper quadrature approximation if a part of the conductor is close to the points of evaluation. This corresponds to cases where the depth of the conductor is small relative to the grid intervals (e.g. only 3 times the grid interval in z). The method used to obviate these difficulties was to refine the grid by a suitable interpolation formula (such as is used for contouring) and integrate on a smaller grid. In all cases, this should be done at least for the top portion of the conductor which is closest to the z=0 plane where the secondary field is evaluated (the plane of the transmitter loop in the case of Turam).

By setting up appropriate tables, the secondary field can be computed along a set of traverses without much more computing time then for a single central traverse. Thus a complete representation of the anomaly on the xy plane can be

easily obtained. It would be just as simple to compute the secondary field at any other location around the conductor, such as may be required for simulation of airborne measurements.

Figures 7 and 8 show the surface anomalies obtained in the cases of the conductors of Figures 5 and 6 respectively. Figure 7 shows the anomaly due to a poor conductor of fairly large size and vertical dip whereas the anomaly of Figure 8 is that of a smaller, dipping, good conductor. The profiles superposed on the central traverses were obtained for the same situations by laboratory model measurements.

The match of the computed and measured anomalies is very good for most curves of Figures 7, 8, and 10. The only exception is the quadrature anomaly of figure 10 (note the expanded scale). The larger relative error in this case is due to the fact that the finite difference approximation does not hold exactly, because the contorted quadrature pattern of Figure 9 would require a smaller grid interval for a proper representation. This is the nature of the poorer accuracy which was discussed above in the cases where the $\sigma\mu\omega tk$ product is large. The condition used for a reasonably good accuracy ($\pm 5\%$ of the % anomaly magnitude) is:

$$\sigma\mu\omega tk \leq 6. \qquad (18)$$

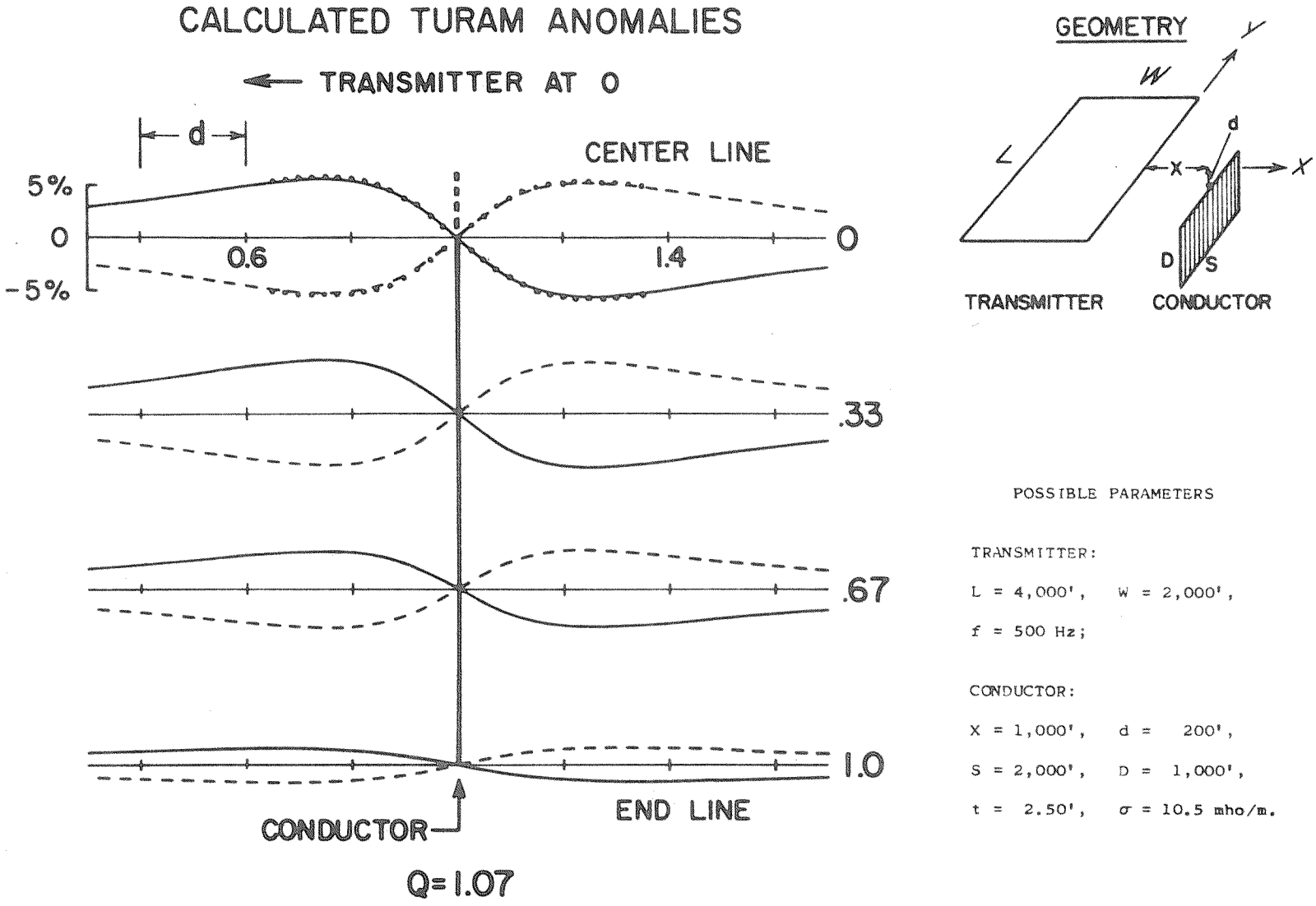

POSSIBLE PARAMETERS

TRANSMITTER:

L = 4,000', W = 2,000',

f = 500 Hz;

CONDUCTOR:

X = 1,000', d = 200',

S = 2,000', D = 1,000',

t = 2.50', σ = 10.5 mho/m.

FIG 7. Surface H_z anomaly caused by the eddy currents of Figure 5. The anomaly recorded by the scale model apparatus in the same situation is shown by the dots superposed on the central profile. Parameters are listed for one possible scale.

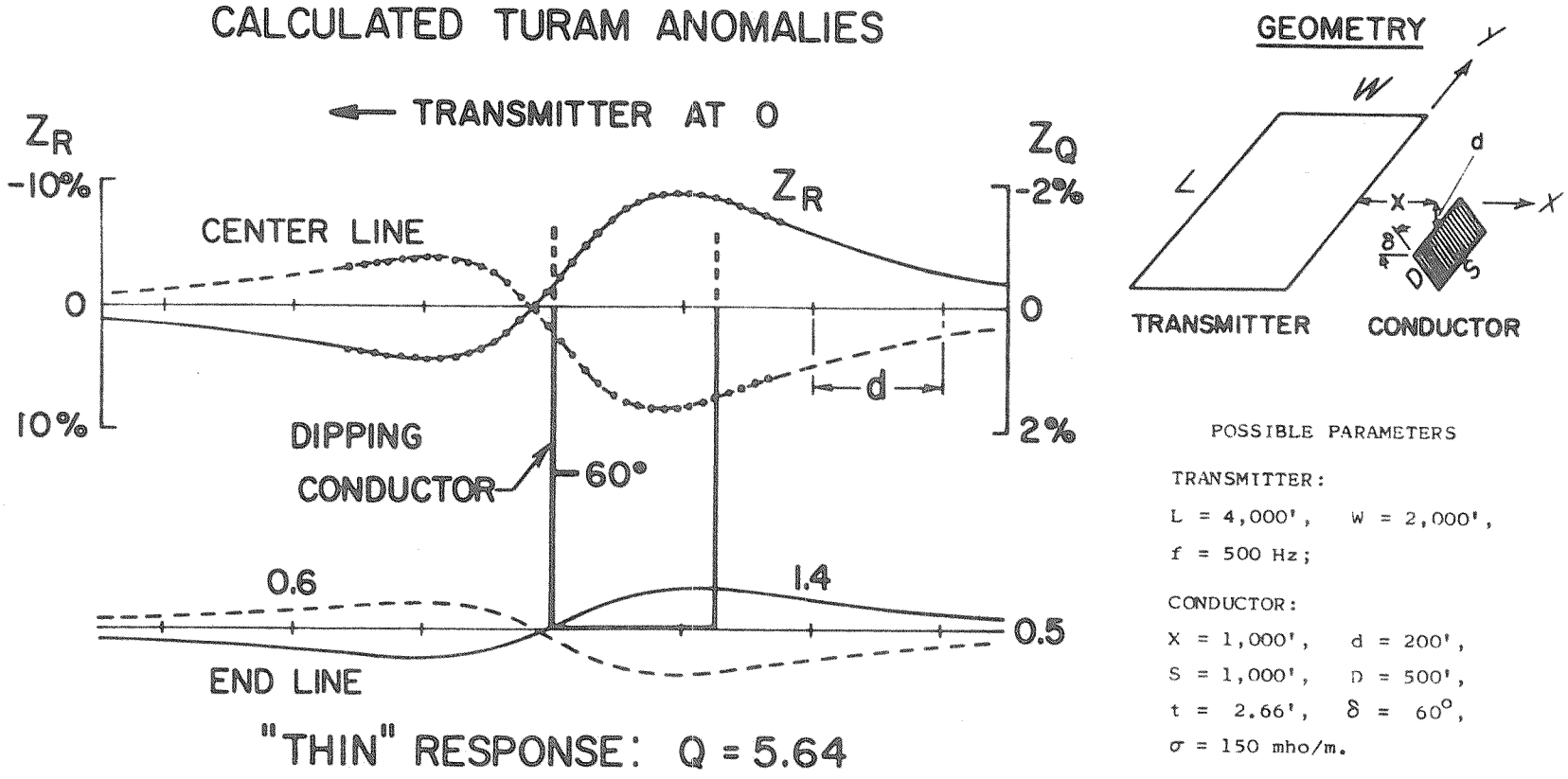

FIG 8. Surface H_z anomaly caused by the eddy currents of Figure 6, with the model and comparison with recorded anomaly as in Figure 7.

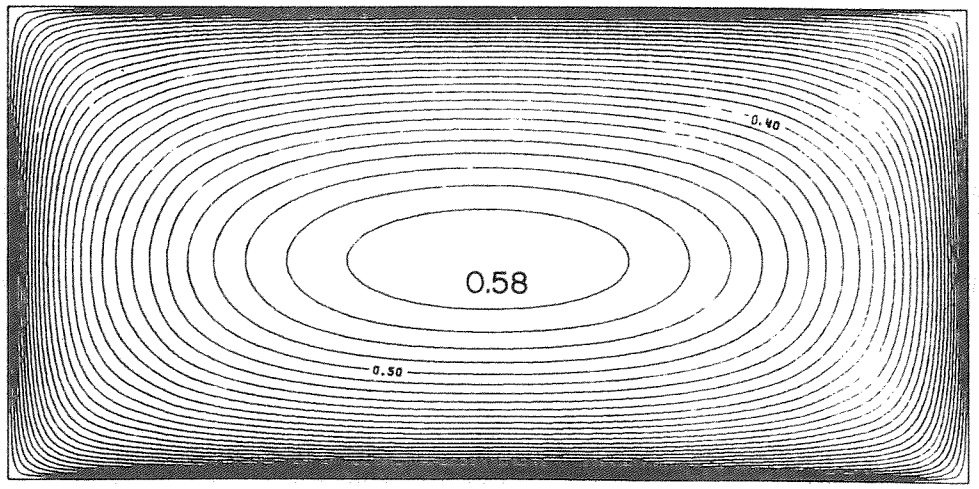

IN PHASE COMPONENT INTERVAL = 0.02 AMP.

EDDY CURRENT PATTERN

COARSE GRID: $\sigma\mu\omega t\Delta = 5.9$ Q = 10.28

QUADRATURE COMPONENT INTERVAL = 0.004 AMP.

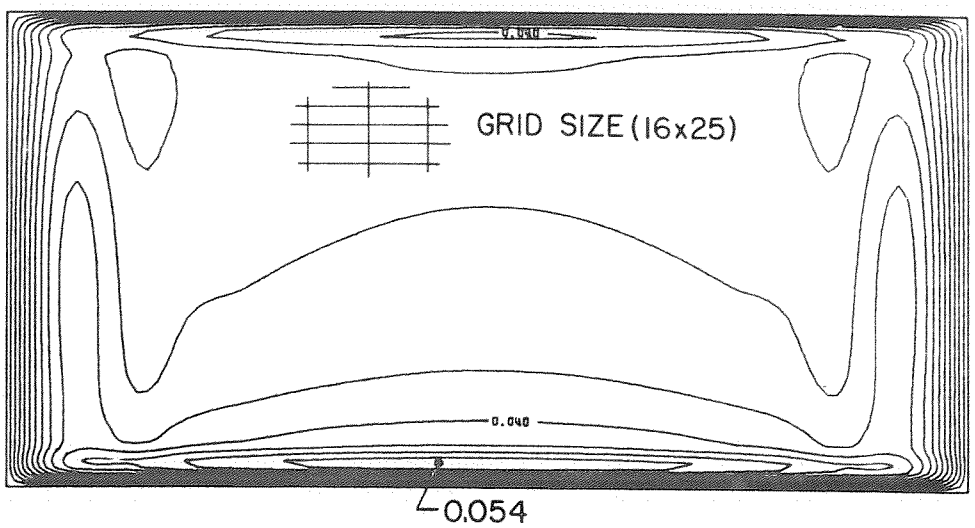

FIG 9. Calculated in phase and quadrature eddy currents inside the conductor shown on the right side of Figure 10. This example illustrates the case when the $\sigma\mu\omega tk$ product becomes large (i.e. when the grid size is too large). The quadrature is more affected because of its more abrupt variations.

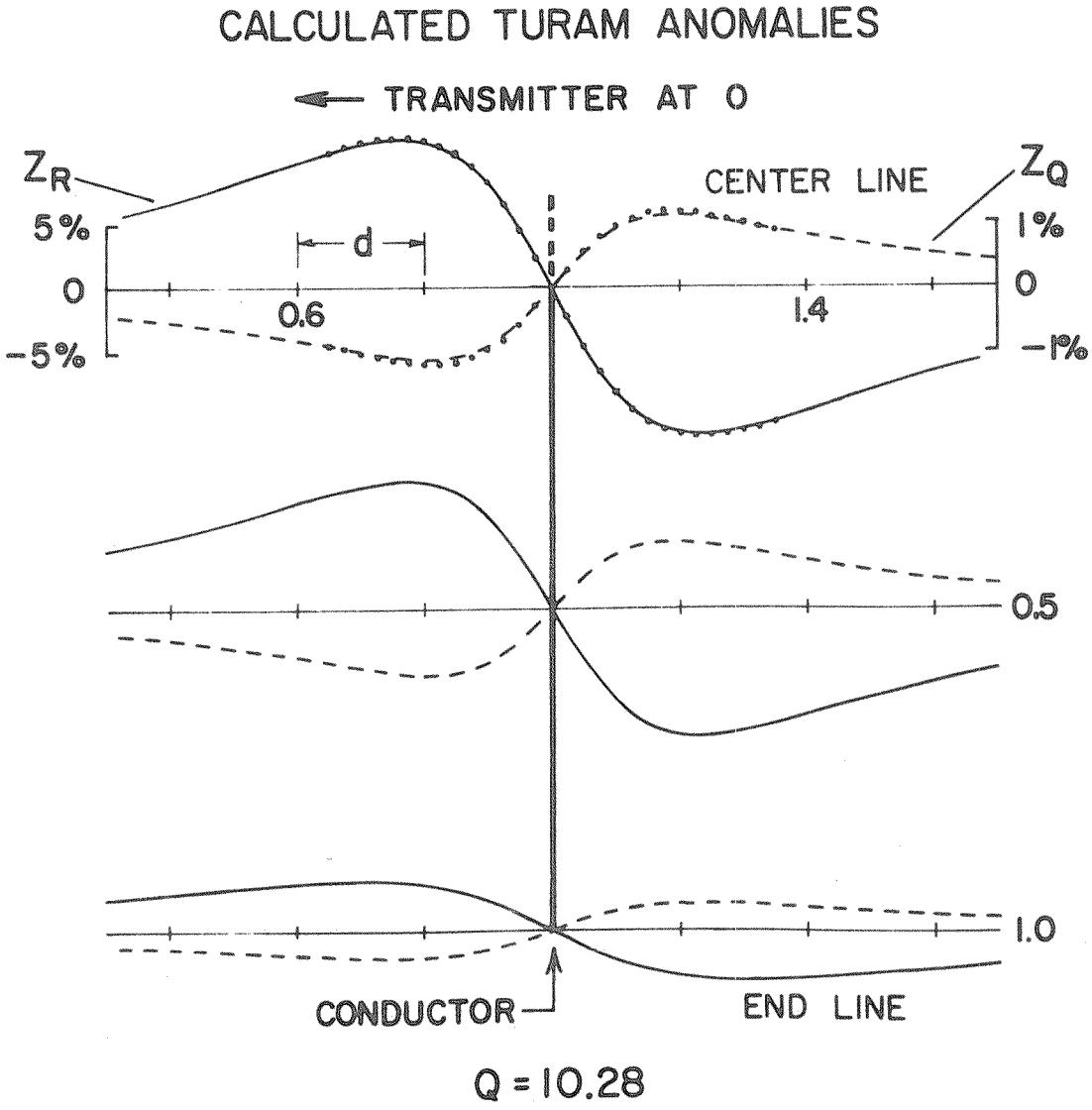

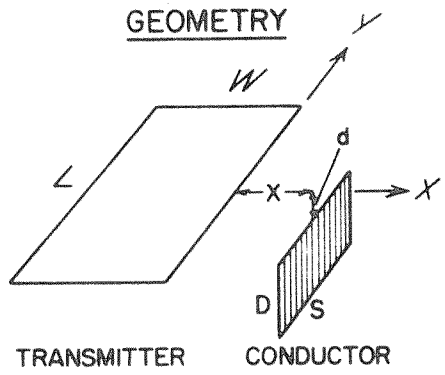

POSSIBLE PARAMETERS

TRANSMITTER:

L = 4,000', W = 2,000',

f = 500 Hz;

CONDUCTOR:

X = 1,000', d = 200',

S = 2,000', D = 1,000',

t = 2.66', σ = 150 mho/m.

FIG 10. The surface H_z anomaly corresponding to Figure 9. The fit of the experimental profile (dots) indicates that the quadrature is relatively more affected by large grid size than the in phase anomaly, resulting in a larger Q (10.28 vs 9.8).

In the example of Figures 9 and 10, the $\sigma\mu\omega tk$ product is 5.9, which means that Figure 10 illustrates about the largest deviation under condition (18). In the product $\sigma\mu\omega tk$, the grid interval k is that of z because it is more critical. In fact, in spite of the larger y dimension of the conductor (2:1), it is possible to use as few as half the number of intervals in y as in z before the stream potential map deteriorates appreciably. Even then, the resulting anomalies show very minor changes and only in the end traverses.

When the condition (18) is respected, the calculated anomalies show a very good accuracy when compared to laboratory measured anomalies. This is illustrated by Figure 11, where the ratios of inphase to quadrature amplitudes (Q ratios) of calculated anomalies have been plotted against the induction number Θ(5) and compared with the experimentally obtained curve. All cases (calculated and measured) correspond to the geometry shown in Figures 7 and 10, and respect the conditions of inductively thin response. For the solutions of best precision (low $\sigma\mu\omega tk$ values), there is a consistent deviation of 5% in Θ which seems to be due to a systematic error in the determination of the conductivities of the plates used as models. The comparison between the calculated and measured

(5) The induction number is defined as $\sigma\mu\omega tL$, L being a length characteristic of the system and depending mostly on the relative and absolute sizes of the conductor and the transmitter (Lamontagne & West, 1971).

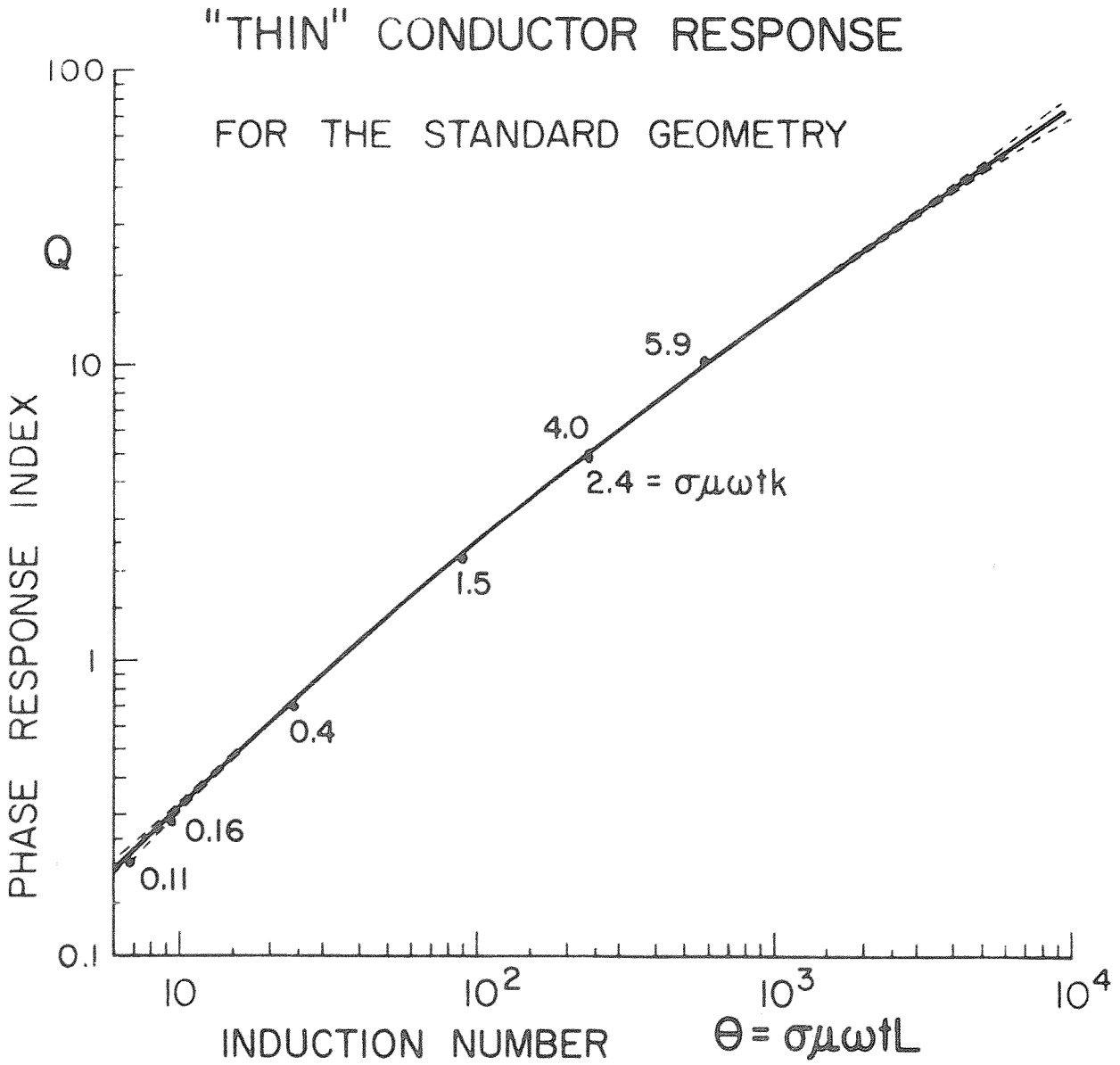

FIG 11. Comparison between the experimental Q vs Θ relationship (solid line) and the Q's of calculated anomalies (dots) for the standard geometry of Figures 7 and 10. The solid line is a polynomial fit of 65 measurements. The dotted lines indicate the belt of 95% confidence on the estimate of Q given Θ. All the anomalies used for this diagram were of inductively thin cases. Superposed on a consistent difference of -5% at low $\sigma\mu\omega tk$ values (best precision), there is a positive deviation in calculated Q's which becomes perceptible at $\sigma\mu\omega tk$ values larger than 2 and which is of +5% at $\sigma\mu\omega tk=6$.

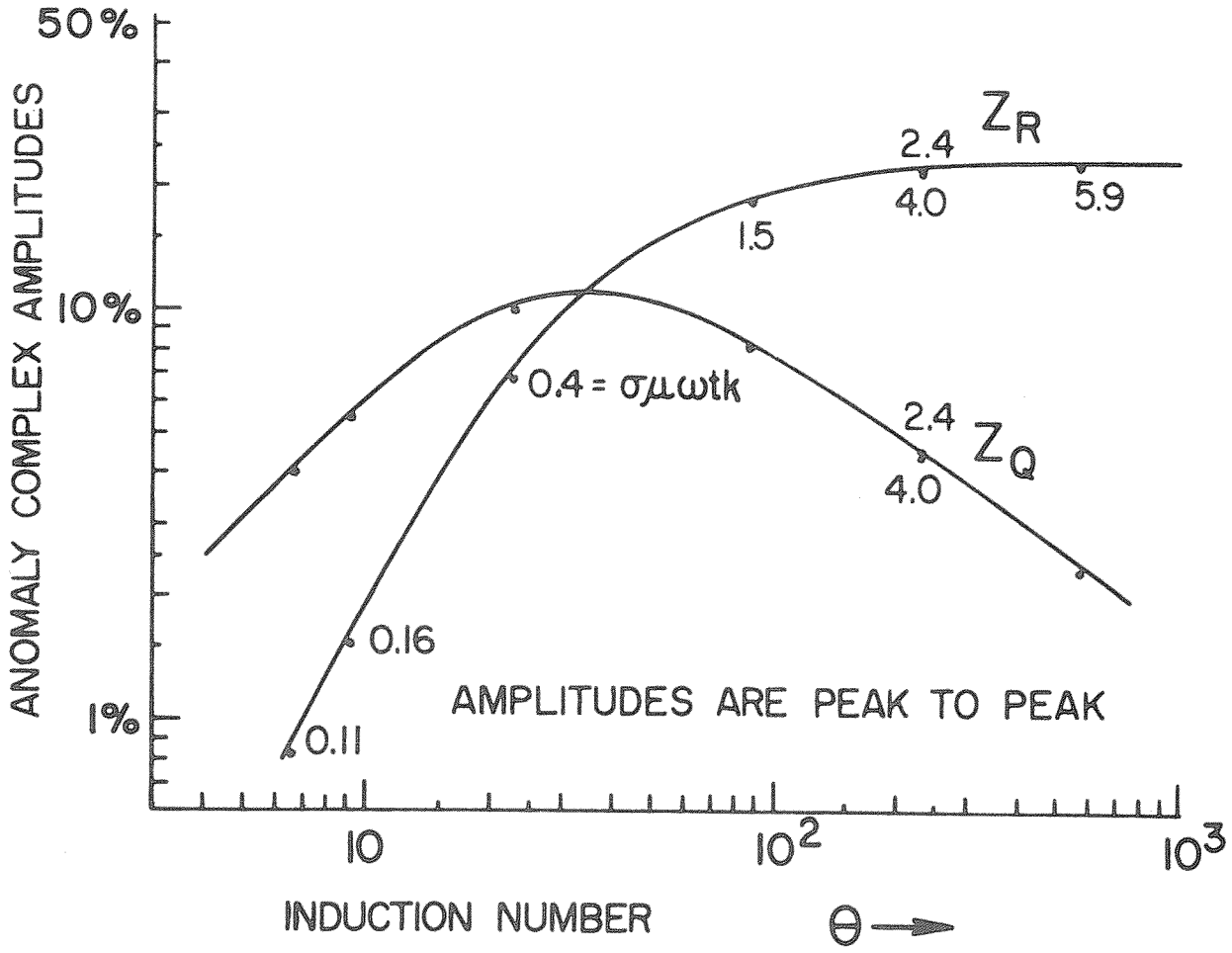

FIG 12. Comparison of the experimental curves of inphase and quadrature amplitudes vs Θ with calculated amplitudes (bases on the same data as Figure 11). The same systematic error in Θ (due to an error in conductivity determination?) shows at low $\sigma\mu\omega$tk values. At high $\sigma\mu\omega$tk (large grid size), the most important deviation occurs on the quadrature component.

amplitudes (Figure 12) indicates the same systematic error and an additional negative deviation due to large grid size ($\sigma\mu\omega tk \geq 2$) mostly affecting the quadrature component, as previously indicated by Figures 9 and 10. Thus the positive Q deviation is due to a negative quadrature deviation (Q = (IN PHASE ampl.)/(QUADR. ampl.).

INDUCTIVELY THICK CONDUCTORS

The finite difference method just outlined can be used only for thin conductors where the current density is uniform across the thickness. This is not always the case, as the classical skin effect may crowd the current towards the surface of the plate. If the current density is non-uniform, a difference in response will be observed.

Let us use the one-dimensional infinite slab model to get an approximate idea of this effect of diffusion. Consider the normal component of the magnetic field H_x. By substituting equation (3) into (7) one obtains, in this simplified case:

$$\frac{\partial^2 H_x}{\partial x^2} = i\sigma\mu\omega H_x$$

for a sinusoidal time dependence. In a case where H_x has the value H_b at both of the boundaries of the slab, the solution

inside the conducting slab is

$$H_x = H_b \frac{\cosh(x\sqrt{i\sigma\mu\omega})}{\cosh(\frac{t}{2}\sqrt{i\sigma\mu\omega})},$$

t being the thickness. In order to get an idea of the effective H_x value, one can find the average of H_x over the thickness:

$$\bar{H}_x = \frac{1}{t}\int_{-t/2}^{t/2} H_x(x)\,dx = H_b \left\{\frac{[\sin 2b + \sinh 2b] + i[\sin 2b - \sinh 2b]}{2b[\cos 2b - \cosh 2b]}\right\}$$

where $b = \frac{t}{2}\sqrt{\frac{\sigma\mu\omega}{2}} = \sqrt{\theta_t/8}$.

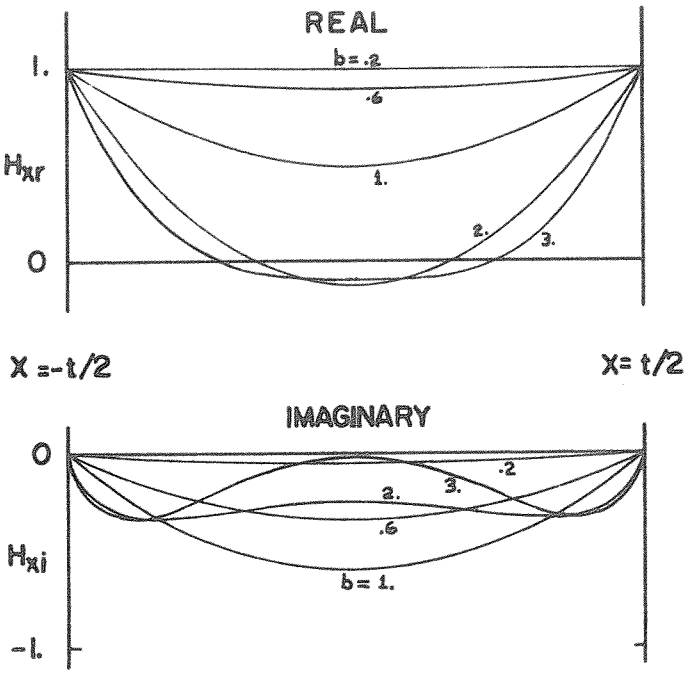

Fig. 13. Diffusion of H_x through an infinite slab of thickness t (one-dimensional case). When the parameter b ($= \frac{t}{2}\sqrt{\frac{\sigma\mu\omega}{2}}$) is large, the H_x alternating field is attenuated and shifted in phase inside the slab. H_x is assumed to have a value H_b of 1.0 at the two boundaries.

As can be seen in Figure 13, when b becomes larger than 0.25, there is an appreciable attenuation of the H_x component. A similar attenuation should occur in the case of a finite tabular

conductor. The equation (13), valid for inductively thin conductors only, can be written

$$\nabla^2 U(y,z) = i\sigma\mu\omega t\, H_b(y,z),$$

where H_b is the x component of the total alternating magnetic field at the boundary (and inside the conductor in the "thin" case).

One way of obtaining an approximation of equation (20) for the case of an inductively thick conductor is to use the $\bar{H}_x/H_b$ ratio obtained from (19) as a multiplicative correction factor on the $H_b(y,z)$ evaluated on the right side of equation (13). The variation of this ratio as a function of b is displayed in Figure 14. This correction method is justified as long as the

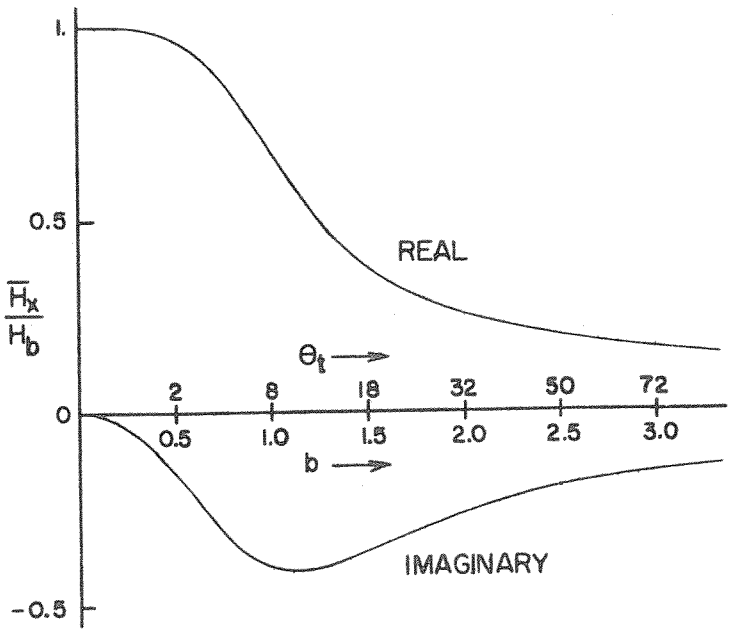

Fig. 14. The average complex attenuation of H_x due to diffusion. The ratio is obtained by integrating H_x over the thickness and dividing by the thickness and the value of H_x at the boundaries, H_b.

important y and z variations of H_x in the conductor occur over much longer lengths than the thickness (i.e. than the length of x variations).

It is possible to obtain approximate solutions of inductively thick problems by including the correction factor in the finite difference equations. But there still remains the condition that the conductors simulated should be geometrically thin. The solutions obtained showed stream potential variations similar to those of inductively thin conductors, except for larger amplitudes and lower Q ratios at equal $\sigma\mu\omega t$ product. This is the qualitative effect that model studies lead us to expect (Bosschart, 1964; Lamontagne & West, 1971). Figure 15 when compared with Figure 6, shows the phenomenon. Both cases have the same $\sigma\mu\omega t$ product and geometry, but Figure 15 corresponds to a thickness 16 times larger than Figure 6 and to b=0.65, a value that is well above the limit for inductively thin conductors (0.25).

In Figure 16, the calculated anomaly of the case of Figure 15 is compared with the anomaly obtained by scale model measurements. It must be noted that the conductor used in the laboratory model was laminated in order to avoid horizontal current loops near the top edge, which affect the quadrature anomaly

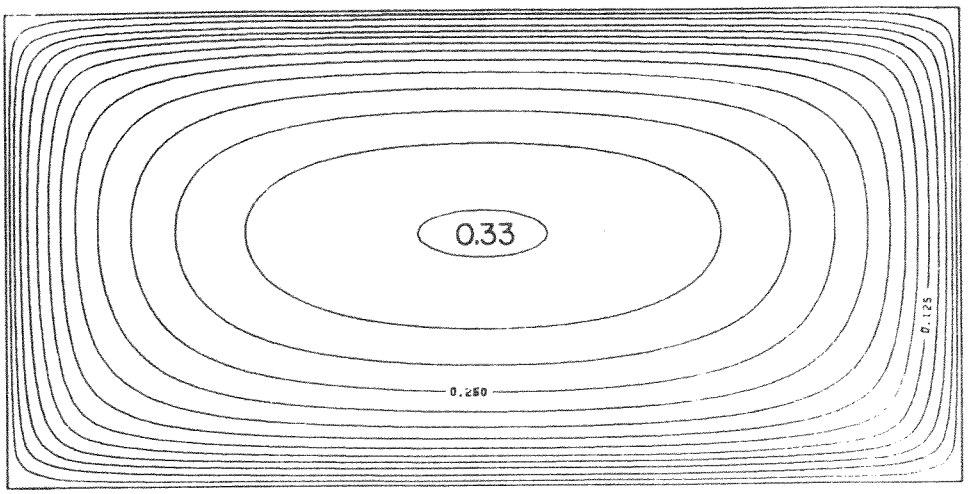

IN PHASE COMPONENT INTERVAL = 0.025 AMP.

EDDY CURRENT PATTERN

"THICK" RESPONSE: Q = 4.55 ("THIN" Q=5.64)

QUADRATURE COMPONENT - INTERVAL = 0.005 AMP.

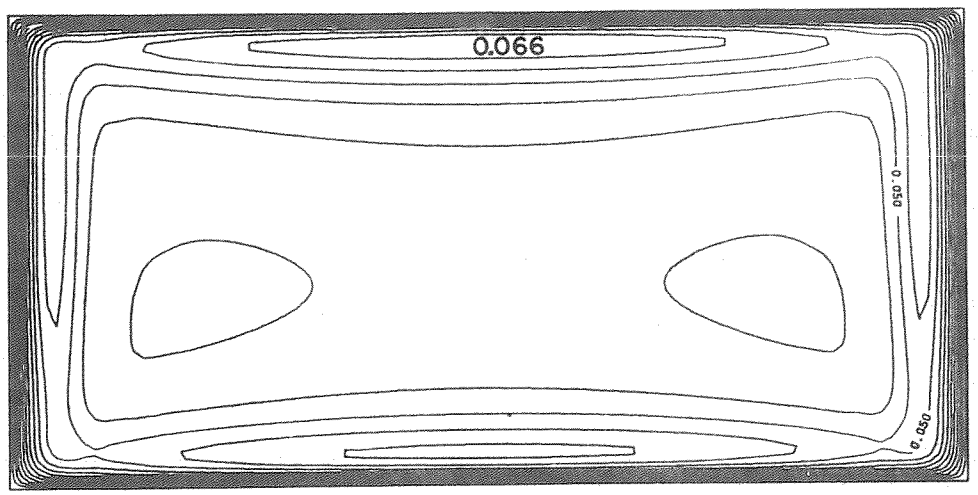

FIG 15. Calculated eddy currents inside the inductively thick conductor shown on the right of Figure 16. The geometry is the same as for the solution of Figure 6, except that the virtual thickness is larger and the conductivity-frequency product is smaller, such as to keep Θ ($=\sigma\mu\omega tL$) constant. This "thick" conductor has larger amplitudes and higher quadrature than the thin conductor of Figure 6.

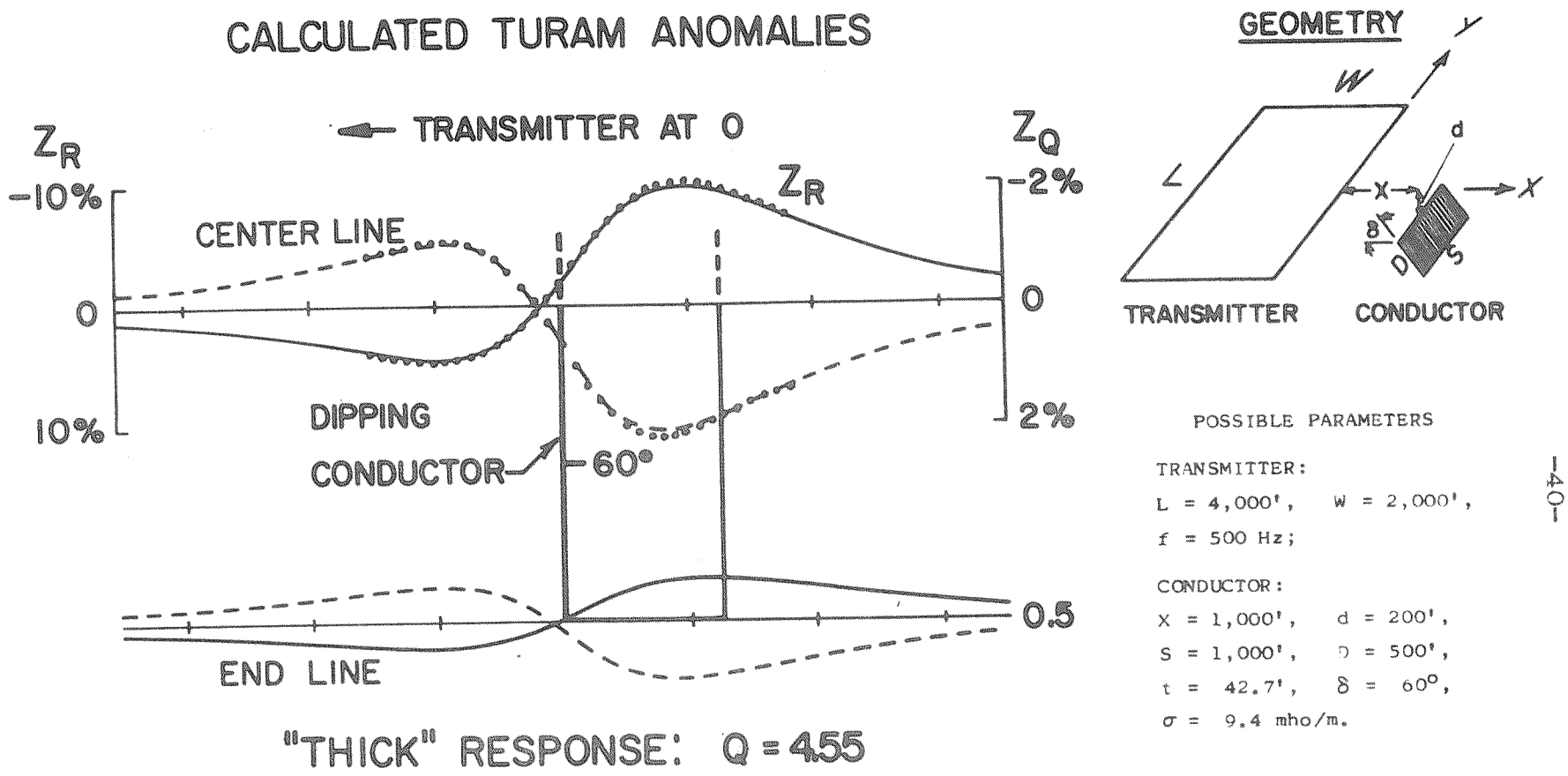

FIG 16. The calculated surface H_z anomaly corresponding to Figure 15. The anomaly has a larger amplitude and a lower Q than that of Figure 8 (same Θ and geometry, but a thin case), which is the qualitative thickness effect expected. But the comparison with the experimental profile on the centre line indicates that the calculated amplitude is too small by 6% in spite of a fairly precise Q (within 2%).

seriously. When compared to Figure 8, it is seen that the calculated anomaly shows qualitatively the right variation in response, i.e. larger amplitude and lower Q. However, the match with the measured profile indicates that the amplitude effect is not quite large enough. On the other hand, the phase response (i.e. the Q ratio) is well reproduced.

Most calculated anomalies of inductively thick conductors, when checked by measurements, compare as well as the above example. Normally the amplitude difference becomes less important when the absolute thickness is smaller. This suggests that a good part of the measured amplitude effect is geometrical, and thus cannot be reproduced in the calculated anomalies in view of the assumption that the conductor is geometrically thin. When the thickness becomes very large (say more than half of the depth), perceptible differences in the Q's of model and calculated anomalies appear as well.

CONCLUSIONS

The numerical solution described permits calculation of the response of thin plates of finite extent, a very useful model in fixed source EM work. For such cases, it can often replace scale model measurements advantageously, since the relative accuracy can be specified by using an appropriate $\sigma\mu\omega t k$ value.

For every solution, the eddy current pattern can be exhibited, thus helping to separate the different effects superposed in measured anomalies.

Without going to an unreasonable number of grid points, and by respecting the condition $\sigma\mu\omega tk \leq 6.0$, anomalies with Q values up to 20 can be calculated with good accuracy. In the cases of inductively thick conductors, there is an additional approximation involved, but if $\sigma\mu\omega tk \leq 6$ and $Q \leq 20$, and if one can assume that the sheet is geometrically thin (thickness $\leq$ 0.3 depth), the calculated anomalies of inductively thick conductors show at most only a small amplitude variation from the measured responses (~8% maximumrelative error).

The method can be modified to calculate the induction in more complex plate models, for instance by using a smoothly varying conductivity specified at the grid points. Alternatively, the virtual thickness could be made variable in a similar fashion. This would make it possible to vary the outline of the plate (within a rectangular limit) by specifying a conductivity or thickness of zero at those grid points which are outside the desired boundary. These modifications would involve only some more computing complications and a small decrease in efficiency, and might be useful in calculating the response of a known geological conductor.

REFERENCES

Bosschart, R.A., 1964, Analytical interpretation of fixed source electromagnetic data (doctoral thesis): U. of Delft, Waltman Publishing Co.

Grant, F.S. and West, G.F., 1965, Interpretation theory in applied geophysics: New York, McGraw-Hill Book Co.Inc., p. 465-470.

Isaacson, E. and Keller, H.B., 1966, Analysis of numerical methods: New York, John Wiley & Sons, Inc., p.66-81.

Lamontagne, Y. and West, G.F., 1971, Conductor thickness effect with the Turam method: Geophysics, in press.

Wait, J.R., 1959, On the electromagnetic response of an imperfectly conducting thin dyke: Geophysics, v.24, p. 167-171.

Wesley, J.P., 1958, Response of thin dyke to oscillating dipole: Geophysics, v. 23, p. 134-143.

West, G.F., 1960, Quantitative interpretation of electromagnetic prospecting measurements (unpublished thesis): U. of Toronto, p. 45-55.